IN SITU CRYSTALLIZATION OF LASER-ACTIVATED METALLIC INKS FOR DIGITAL INKJET PRINTING

E. Ferrer[1], *A. Lahlahi*[1], *J. B. Carda*[1]

[1] Department of Inorganic Chemistry, Universitat Jaume I (UJI), Avenue Vicent Sos Baynat, s/n, 12006 Castellón de la Plana, Spain, al404110@uji.es

Summary: This study presents a novel technique for enhancing ceramic decoration through inkjet printing by developing laser-activated metallic inks. This method consists of crystallizing metallic layers directly on ceramics using inks containing copper, nickel, or cobalt acetates. Pulsed laser irradiation at 1064 nm produces a metallic layer integrated into the glassy surface matrix. Scanning Electron Microscopy (SEM) shows integrated spherical structures with diameters smaller than 350 nm. The observed reflectance effect, indicated by UV-vis diffuse reflectance spectroscopy, is due to the resonant effects of surface plasmons of nanosized metal particles. Transmission Electron Microscopy (TEM) confirms the presence of crystals of approximately 20 nm. X-Ray diffraction analysis (XRD) confirms the laser-induced redox transformation of Cu (II), Ni (II) and Co (II) precursor acetates into reduced Cu (0), Ni (0) and Co (0) nanoparticles. The results of the Selected Area Electron Diffraction analysis (SAED) supports these findings. This pioneering approach holds great potential for advancing digital ceramic decoration techniques.

Keywords: Direct Laser Writing, Digital printing, Inks, Metallic film, Ceramic functionality.

1. INTRODUCTION.

Advanced laser technologies have opened new perspectives in surface processing, enabling the creation of micro- and nanoscale structures with wide-ranging functional applications. These laser-activated surface structures have significantly enhanced the performance of devices in sectors such as optics, electronics, and biomedicine. Among others, one of the recent areas under strong research interest involves laser-induced surface coloration, which affects optical properties due to modulation of light reflection, interference, and scattering on metallic and ceramic substrates [1]. This innovation has notable implications for industries ranging from solar energy, where laser techniques improve light absorption efficiency, to digital decoration processes like inkjet printing.

The ceramic tile industry has embraced these laser-activated advancements within the last years [2]. From traditional decoration methods to high-definition digital inkjet printing, new challenges and opportunities opened up, particularly in the development of inks capable of sustaining the demands of laser-assisted applications. Traditionally, the processing of ceramic pigments involved high-temperature and energy-intensive processes; however, sustainability concerns and advancements in laser processing have prompted research into alternative pigment formulations, including the use of metallic inks activated by laser energy [3]. These metallic inks offer unique advantages such as wear resistance and metallic effects ideal for durable customized surfaces [4].

2. METHODOLOGY.

The methodology followed in the experimental procedure is based on three inks of Cu, Ni and Co, which must be crystallized using laser technology. During this process, the ink composition, beam irradiance, and beam scanning type must be optimized, following this order, using XRD in each optimization. Once the samples are optimized, they are characterized separately using various techniques such as SEM, TEM, EDX and UV-Vis.

3. EXPERIMENTAL PROCEDURE.

3.1. Materials and methods.

The raw materials used to prepare copper, nickel and cobalt metallic inks by metal-organic decomposition were copper acetate ($(CH_3COO)_2Cu{\cdot}H_2O$) from AppliChem (98 % purity), nickel acetate ($(CH_3COO)_2Ni{\cdot}4H_2O$) from Merck (98 % purity), cobalt (II) acetate ($Co(CH_3CO_2)_2{\cdot}4H_2O$) from Merck (98 % purity), ceramic frit, branched polyethyleneimine (97 % purity) with medium Mw ~1200 g/mol as complexing and reducing agent as well as rheological agent adjusting the ink viscosity. High purity isopropanol was used as solvent.

A Raycus RFL-P120MX model pulsed fiber laser was used to decompose the deposited precursor. This equipment operates at a fundamental wavelength of 1064 nm. The scanning direction of the laser beam was controlled using a galvanometric scanner and focused using an f-theta telecentric lens (f = 100 mm), allowing coverage of areas larger than 25 cm^2 on the sample and surface scanning speeds ranging from 10 to 3000 mm/s. The diameter of the focused beam was 54 µm ($1/e^2$) on the surface. This equipment is a 120 W MOPA fiber

laser that uses Master Oscillator Power Amplification technology. The parameters have been calibrated with a thermal sensor whose model is F150(200)A-CM-16.

3.2. Preparation of metallic ink.

The metallic ink is distinguished in two parts: solid part and liquid part. On one hand, the solid phase includes copper, nickel, and cobalt acetate as metallic precursors. It also contains a prepared frit that will be the vitrifying part for the metallic layer to integrate into the ceramic substrate. On the other hand, the ink has a liquid phase that functions as a vehicle for the previous phase. 5 g of the solid phase (the amount of each depending on the ratio Metal:Frit) was dispersed in 1 mL of isopropyl alcohol (IPA), which will be the solvent. Additionally, 1 drop of polyethyleneimine (PEI) was added, which is a polymer containing C and N and induces the formation of a Cu, Ni and Co coordination polymer with a high stability constant. The composition of Cu, Ni and Co inks can be seen in *Table 1*. Therefore, this polymer acts as both a reductant and a rheology modifier (step 1). The resulting viscous ink was applied using a doctor blade onto a ceramic substrate containing a glaze based on the same frit composition (step 2). The deposited ink was kept under an IR lamp for 10 minutes to dry (step 3). This prepared layer will be crystallized by laser radiation (step 4).

Table 1. Metallic ink compositions studied.

Reference	Acetate (g)	Frit (g)	Ratio Metal:Frit	PEI (drops)	IPA (mL)
Cu-100	0.5	0	1:0	1	1
Cu-50	0.25	0.25	1:1	1	1
Cu-20	0.1	0.4	1:4	1	1
Cu-10	0.05	0.45	1:10	1	1
Ni-100	0.5	0	1:0	1	1
Ni-50	0.25	0.25	1:1	1	1
Ni-20	0.1	0.4	1:4	1	1
Ni-10	0.05	0.45	1:10	1	1
Co-100	0.5	0	1:0	1	1
Co-50	0.25	0.25	1:1	1	1
Co-20	0.1	0.4	1:4	1	1
Co-10	0.05	0.45	1:10	1	1

3.3. Laser digital patterning process.

On the one hand, to optimize laser conditions, different power levels (12, 24, 36 and 60 W) have been studied for copper, nickel, and cobalt samples. In the three cases, the scanning speed of the beam has been 2000 mm/s. However, the pulse frequency and duration have been different. For the copper sample, it was 1000 kHz and 17 ns, and for the nickel layer, it was 500 kHz and 100 ns and for the cobalt layer, it was 1000 kHz and 100 ns. *Table 2* shows the irradiance and fluence values for each experiment.
On the other hand, the type of scanning used in laser deposition is crucial for the crystallization of the metal layer. Bidirectional Continuous (BDC) scanning, where the laser beam scans in both directions without stopping, promotes a uniform advancement of the molten front by preventing cooling at the line change. In contrast, Bidirectional Discontinuous (BDD) scanning involves the laser pausing at the end of each line before changing direction, which can influence the deposition process and affect the final crystallization.

Table 2. Summary of irradiance and fluence values for experiments on copper, nickel and cobalt layers.

Reference	Irradiance (MW/cm^2)	Fluence (J/cm^2)
Cu-12W	30.82	0.52
Cu-24W	61.64	1.05
Cu-36W	92.47	1.57
Cu-60W	154.11	2.62
Ni-12W	10.48	1.05
Ni-24W	20.96	2.10
Ni-36W	31.44	3.14
Ni-60W	52.40	5.24
Co-12W	5.24	0.52
Co-24W	10.48	1.05
Co-36W	15.72	1.57
Co-60W	26.20	2.62

4. RESULTS AND DISCUSSION.

4.1. Film optimization by XRD.

After synthesizing and depositing the Cu, Ni and Co inks, they must be crystallized using laser technology. Parameters that depend significantly on crystallization should be optimized by X-ray diffraction, such as ink composition, irradiance, and type of scanning.
In this section, the crystallographic analysis of the films will be carried out according to their composition in *Figure 1 (a, b, c)*, the optimum irradiance in *Figure 1 (d, e, f)* and the optimum scan type in *Figure 1 (g, h, i)*. Each figure has 3 sections corresponding to the Cu (a), Ni (b) and Co (c) film.
This section analyses the crystal structures of copper, nickel, and cobalt films based on data from the International Centre for Diffraction Data (ICDD). Copper, with ICDD card [00-003-1005], has an FCC structure with a lattice parameter of 3.607 Å, and diffraction peaks at angles 2θ, 43.40 º and 50.55 º, corresponding to (111) and (200) planes. Nickel, from ICDD card [00-004-0850], also has an FCC structure with a 3.523 Å lattice parameter, showing diffraction at 2θ, 44.50 º and 51.95 º. Similarly, cobalt, according to ICDD card [00-015-0806], has an FCC structure with a lattice parameter of 3.5447 Å, and peaks at 2θ, 44.50 º and 51.95 º, corresponding to the (111) and (200) planes.

4.1.1. Effect of ink composition.
Regarding the optimization of the ratio (Metal:Frit), the differences in intensities between the peaks of the specific metal can be observed depending on the ink composition, as seen in *Figure 1 (a, b, c)*.
It is noted that all Cu and Co inks (a, c respectively) behave in the same way. The 1:0 ratio results in the desired crystalline phase but lacks adhesion, while the 1:10 and 1:4 ratios improve adhesion but do not crystallise the important peaks (111 and 200). In the case of Ni ink, no crystalline phase is observed with a 1:0 or 1:10 ratio due to poor adhesion, but with a 1:4 ratio partial crystallisation occurs. Complete reduction

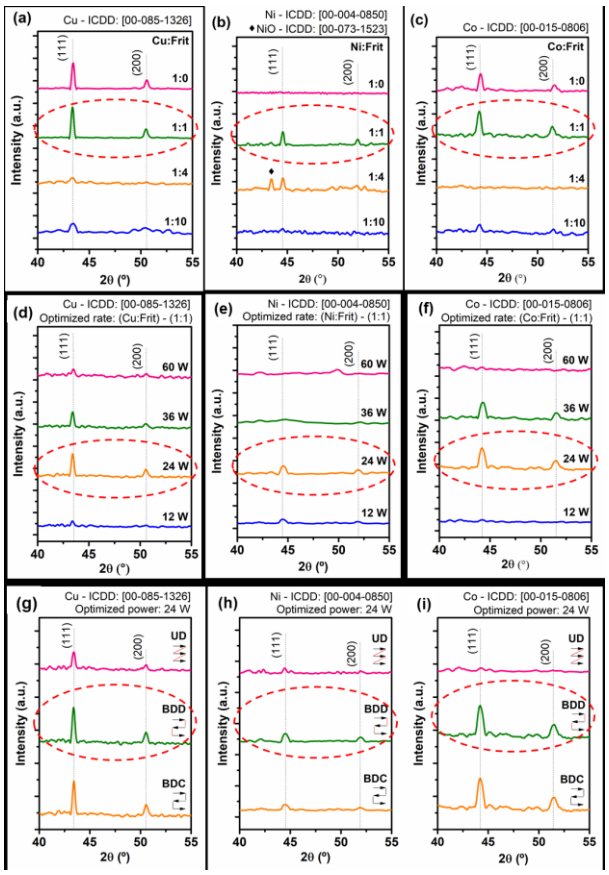

Figure 1. XRD of Cu ink (a), Ni ink (b) and Co ink (c) irradiated at different compositions of the metal; XRD of Cu-50 (d), Ni-50 (e) and Co-50 (f) samples irradiated at different irradiances; and XRD of Cu-50-24W (g), Ni-50-24W (h) and Co-50-24W (i) samples.

and the desired crystalline phases are achieved with a 1:1 ratio in all cases, which gives optimum adhesion and crystallisation.

4.1.2. Effect of laser irradiance.

After optimizing the ratio (Metal:Frit), the laser irradiance must be optimized, since it is a parameter that can significantly vary the crystallization of the metal film. Hence, *Figure 1 (d, e, f)* shows the different diffractograms varying the power at 12 W, 24 W, 36 W and 60 W, but shown together with their respective irradiance and fluence (as indicated in *Table 2*).

Visualizing these graphs, the behaviour is the same in the three cases. At a power of 12 W, hardly any metal has crystallized, whereas when the power is increased to 24 W, the peaks corresponding to the metal are more intense. However, if the power is increased further, at 60 W power, the metallic film is being stripped off, so the crystalline structure is stripped off, and the amorphous structure would predominate.

Based on the results obtained, for the study of copper, nickel and cobalt films, the power has been optimized at 24 W, whose irradiances are 62 MW/cm^2, 21 MW/cm^2 and 10 MW/cm^2, respectively.

4.1.3. Effect of scanning type.

To optimise the ink by XRD, the scanning direction of the laser must be considered, as it significantly influences the crystallisation. Three types of scanning were examined: bidirectional continuous (BC), bidirectional discontinuous (BD) and unidirectional (UD). The behaviour is seen in *Figure 1 (g, h, i)* for Cu. Ni and Co films, respectively.

In the case of copper films, all scanning types produced crystallisation, while BD provided the highest degree of crystallisation. In contrast, nickel and cobalt films showed minimal crystallinity with the UD scanning due to rapid cooling during non-irradiated returns. Bidirectional scanning, both continuous and discontinuous, stabilised the molten zones, improving crystallinity, although BC occasionally caused edge defects.

Finally, bidirectional scanning, especially BD, was optimal for crystallisation.

Once this optimisation has been completed, characterisation of the copper, nickel and cobalt films will be carried out using other techniques.

4.2. Nanostructural analysis using electron microscopy.

SEM micrographs of the copper, nickel and cobalt layers reveal different surface characteristics. The copper layer (*Figure 2 (a)*) has nanometre-sized spherical particles, ranging in size from 50 to 350 nm and averaging 150 nm in size, which cause plasmonic effects that give the layer a blue colour. The nickel layer (*Figure 2 (b)*) has smaller, spherical, adherent particles embedded in a glassy matrix, with sizes ranging from 10 to 225 nm and an average of 125 nm. In contrast, the cobalt layer (*Figure 2 (c)*) has randomly dispersed irregular particles, with an average size of 90 nm. All layers show plasmonic resonances due to their high surface-to-volume ratio, which influences light absorption and colour.

In addition, energy dispersive X-ray analysis (EDX) has been carried out, showing the metallic composition of each layer (Cu, Ni and Co).

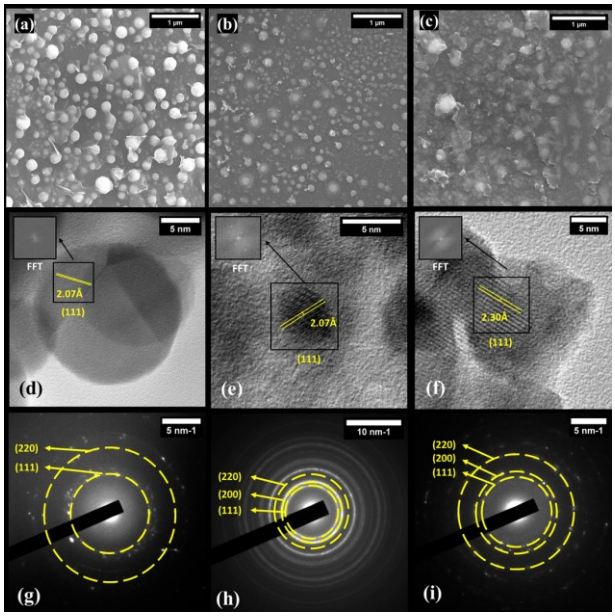

Figure 2. SEM micrographs of Cu-50-24W (j), Ni-50-24W (k) and Co-50-24W (l) samples; and HRTEM images and ring diffraction patterns of Cu-50-24W (m, p), Ni-50-24W (n, q) and Co-50-24W (o, r) samples.

The study used high-resolution transmission electron microscopy (HRTEM) and selected area electron diffraction (SAED) to analyse the morphology and crystallinity of laser-crystallised copper, nickel and cobalt nanoparticles. HRTEM images revealed clear crystallographic planes, with the Inverse Fourier Transform (IFFT) identifying the (111) plane with an interplanar spacing of 2.07 Å in both copper (*Figure 2 (d)*) and nickel (*Figure 2 (e)*) samples. SAED patterns of Cu and Ni (*Figure 2 (g) and (h)*, respectively) confirmed the highly crystalline structure of the nanoparticles, showing well-defined diffraction rings for both the (220) and (111) planes.
Furthermore, in the case of the cobalt layer, HRTEM image, seen in *Figure 2 (f)*, identified a cobalt metal structure with an interplanar distance of 2.30 Å for the (111) plane. SAED patterns (*Figure 2 (i)*) confirmed the highly crystalline structure of the cobalt nanoparticles, showing distinct diffraction rings for the (220), (200) and (111) planes.
Other observed rings, of *Figures 2 (g), (h) and (i)*, were attributed to frit phases, which were not the focus of the study.

4.3. Optical properties analysis.

The glazed ceramic obtained after laser treatment exhibited a continuous, coloured, and metal-like surface appearance, as observed in *Figure 3*, where on one side, a sample of copper ink treated (Cu-50) at 31, 62, 92, and 154 MW/cm^2 is shown in *Figure 3 (a)*; on the other side, a sample of nickel ink (Ni-50) is displayed in *Figure 3 (b)*, illustrating the layers obtained by irradiating at 10, 21, 31, and 52 MW/cm^2; in addition, below in *Figure 3 (c)*, the treated cobalt ink (Co-50) is observed at 5, 10, 16 and 26 MW/cm^2. These images clearly show the laser-treated areas on the metallic squares as well as the deep blue raw copper ink layer, the light blue raw nickel ink layer and the red raw cobalt ink layer. The original surface of the white glazed tile is also observed. The laser beam was scanned continuously bidirectionally, although the images also show the results obtained by scanning unidirectionally or discontinuously bidirectionally.

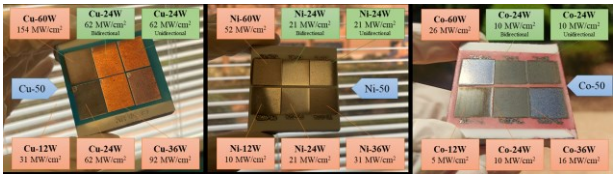

Figure 3. Image of irradiated ink with different values of laser irradiance and different types of scanning (a) Cu-50, (b) Ni-50 and (c) Co-50 samples.

UV-visible spectroscopy is used to analyse, the treated layers can be explained better with absorbance spectra. The typical maximum absorbance of Cu, Ni and Co are 450, 350 and 400 nm, respectively; with these bands, the coloration can be explained by the effect of plasmon resonance [5].

5. CONCLUSIONS.

After carrying out this project on the synthesis, deposition and crystallization of copper, nickel and cobalt coatings using laser operating at 1064 nm. It becomes evident how this laser coating method offers advantages over traditional pigment inks, requiring much less energy and time. Furthermore, it is a fully scalable industrial process, eliminating the need for thermal treatments for the ink components.
Firstly, X-ray diffraction (XRD) has confirmed the crystallization of single metallic phases of Cu, Ni and Co.
Secondly, by SEM, it is observed that the average particle size of Cu, Ni and Co films: 120, 120 and 90 nm. Furthermore, by HRTEM, crystal sixes of less than 20 nm are observed whose interplanar distances correspond to the metallic phases of Cu, Ni and Co, promoting plasmon resonance effects.
In addition, UV-Vis spectroscopy of the ink identifies the absorption band of the metallic nanoparticles.

6. FUTURE LINES OF RESEARCH.

This research project explores a new area, opening up several future study directions. First, the composition of metallic inks will be improved by incorporating new metals or alloys to enhance their physical and chemical properties, and by modifying ink rheology to increase deposition precision in inkjet printing.
Furthermore, an investigation into the electrical and optical properties of crystalline metallic layers will assess their performance in various technological applications.
Finally, the research will be applied to emerging technologies, such as printed electronics, medical device manufacturing, the automotive industry, and energy applications like printed solar cells and flexible batteries, along with advancing ceramic functionalities.

7. REFERENCES.

[1] Liu, H.; Lin, W.; Hong, M. Surface Coloring by Laser Irradiation of Solid Substrates. APL Photonics 2019, 4 (5). https://doi.org/10.1063/1.5089778.
[2] Atılgan Türkmen, B.; Karahan Özbilen, Ş.; Budak Duhbacı, T. Improving the Sustainability of Ceramic Tile Production in Turkey. Sustain Prod Consum 2021, 27, 2193–2207. https://doi.org/10.1016/J.SPC.2021.05.007.
[3] Enríquez, E.; Reinosa, J. J.; Fuertes, V.; Fernández, J. F. Advances and Challenges of Ceramic Pigments for Inkjet Printing. Ceram Int 2022, 48 (21), 31080–31101. https://doi.org/10.1016/J.CERAMINT.2022.07.155.
[4] Wu, Q.; Long, W.; Zhang, L.; Zhao, H. A Review on Ceramic Coatings Prepared by Laser Cladding Technology. Optics and Laser Technology. Elsevier Ltd September 1, 2024. https://doi.org/10.1016/j.optlastec.2024.110993.
[5] Wapnir, R. A. Copper Absorption and Bioavailability. Am. J. Clin. Nutr. 1998, 67 (5), 1054S-1060S. DOI: 10.1093/ajcn/67.5.1054s.